Journal of Photochemistry and Photobiology A: Chemistry 210 (2010) 145–152

Contents lists available at ScienceDirect

Journal of Photochemistry and Photobiology A: Chemistry

journal homepage: www.elsevier.com/locate/jphotochem

TiO_2- and ZnO-based solar cells using a chlorophyll *a* derivative sensitizer for light-harvesting and energy conversion

Xiao-Feng Wang[a,b,*], Osamu Kitao[a], Eiji Hosono[a], Haoshen Zhou[a,**], Shin-ichi Sasaki[c,d], Hitoshi Tamiaki[d]

[a] *Energy Technology Research Institute, National Institute of Advanced Industrial Science and Technology (AIST), Umezono 1-1-1, Tsukuba, Ibaraki 305-8568, Japan*
[b] *Environmental and Renewable Energy Systems Division, Graduate School of Engineering, Gifu University, Yanagido 1-1, Gifu 501-1193, Japan*
[c] *Nagahama Institute of Bio-Science and Technology, Nagahama, Shiga 526-0829, Japan*
[d] *Department of Bioscience and Biotechnology, Ritsumeikan University, Kusatsu, Shiga 525-8577, Japan*

ARTICLE INFO

Article history:
Received 30 August 2009
Accepted 8 January 2010
Available online 15 January 2010

Keywords:
Chlorophyll
Dye-sensitized solar cell
Zinc oxide nanomaterials
DFT calculations

ABSTRACT

TiO_2- and ZnO-based solar cells sensitized by a chlorophyll *a* derivative (methyl *trans*-3^2-carboxypyropheophorbide *a*) were fabricated and compared. The TiO_2-based solar cell produces higher values for the short-circuit photocurrent (J_{sc}), open-circuit photovoltage (V_{oc}), and energy-to-electricity conversion efficiency (η) than the ZnO-based solar cell. The observed ATR-FTIR data on the dye-sensitized semiconductor electrodes and the spectra estimated from the density functional theory (DFT) suggest that the dye sensitizer is bound to TiO_2 with both the bidentate chelating and monodentate modes but is bound to ZnO with the monodentate mode exclusively. The frontier orbitals of the dye molecule bound to semiconductors suggest that the HOMO-2 and LUMO + 2 orbitals of the dye sensitizer do not participate in electron transfer processes for the dye–ZnO system, resulting in a lower J_{sc} value and a relatively narrow response for the incident photon-to-current conversion efficiency in the solar cell. Transition component analysis based upon the time-dependent DFT results explains well the experimental UV–vis spectra and difference in the η values between the dye-sensitized solar cells based upon TiO_2 and ZnO nanocrystalline electrode materials.

1. Introduction

Since the historic paper on dye-sensitized solar cells (DSSCs) published in 1991 by Prof. M. Grätzel, DSSCs have quickly attracted great attention from people in various fields due to their low cost and wide scientific interests [1,2]. The solar energy-to-electricity conversion efficiency (η) for the best DSSCs has now been enhanced from 7.1% to 11%, with various recent efforts directed mainly towards developing better inorganic electrode materials and organic sensitizers [3,4]. TiO_2 and ZnO are commonly regarded as the most promising electrode materials for DSSCs due to their wide band gaps, which are suitable for interfacial electron transport to take place. In terms of solid state physics – band gap, band energy, etc. – ZnO-based DSSCs should perform almost equally well as corresponding TiO_2-based DSSCs [5,6]. Compared to TiO_2, ZnO as an electrode has even more advantages:

1. The ZnO morphology is much easier to control.
2. The ZnO layer can be crystallized at lower temperatures, which is useful in flexible-type DSSCs based upon plastic substrates.
3. ZnO has better electron mobility [7–9].

However, DSSCs based upon ZnO materials composed of nanostructures – nanoparticles, nanowires, nanosheets, and aggregates – still have limited ηs less than 7% [10–13]. The lower ηs of ZnO-based DSSCs have mainly been attributed to the ready formation of multilayer dye aggregation on ZnO surface when the ruthenium complexes N3 or N719, with more than two carboxy groups, are employed as sensitizers [14]. This is a weak explanation because the ZnO-based solar cells show lower ηs even at a lower dye concentration and in circumstances with a far less chance of aggregate formation [15,16]. An alternative explanation for the lower η is the possibly inefficient electron injection process at the dye–ZnO interface [17]. However, there is no direct evidence supporting this explanation. In actuality, the electron injection time for the dye–ZnO colloid system can be as short as 190 fs, suggesting strong electronic coupling between the dye and the ZnO electrode [18].

* Corresponding author at: Environmental and Renewable Energy Systems Division, Graduate School of Engineering, Gifu University, Yanagido 1-1, Gifu 501-1193, Japan. Tel.: +81 080 3534 8690; fax: +81 58 293 2594.
** Corresponding author. Fax: +81 29 861 5799.
E-mail addresses: charles1976110@hotmail.com (X.-F. Wang), hs.zhou@aist.go.jp (H. Zhou).

1010-6030/$ – see front matter © 2010 Elsevier B.V. All rights reserved.
doi:10.1016/j.jphotochem.2010.01.004

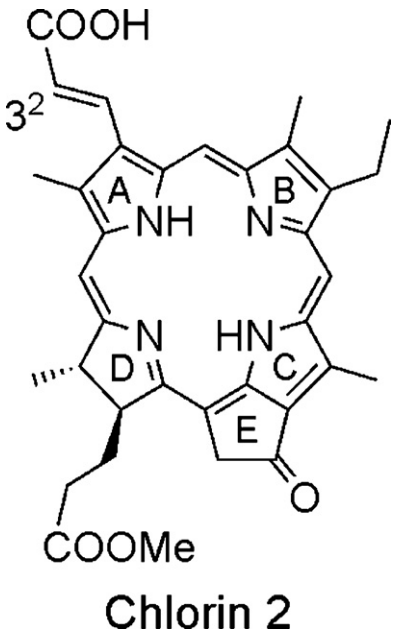

Fig. 1. The chemical structure of the dye sensitizer chlorin 2.

The binding modes of dye sensitizers with TiO_2 have been extensively studied, but little knowledge about the binding modes for dye sensitizer with ZnO is available [19,20]. Some sensitizers, such as ruthenium complex N3 and Zn(II) tetraarylporphyrins, tend to bind with TiO_2 and ZnO in similar ways [21,22]. However, for dye sensitizers with longer conjugated chains, the binding modes of their carboxy group with TiO_2 and ZnO are not necessarily identical. For example, all-*trans*-retinoic acid can bind to TiO_2 through not only ester but also chelating and bridging formations [23]. It is naturally expected, therefore, that electronic coupling and electron injection at the dye–semiconductor interface should be different when dye sensitizers are bound to TiO_2 and ZnO surfaces in different binding modes.

Compared to the N719 dye, the organic dye sensitizer D149 was introduced in ZnO-based DSSCs exhibiting a better incident photon-to-current conversion efficiency (IPCE) value at the absorption maximum [24,25]. The resulting photocurrent of the D149-sensitized ZnO solar cell was still low and mainly originated from the limited light-harvesting capability of the dye on ZnO films. Therefore, organic dye sensitizers with excellent light-harvesting capability are highly desired for the study of ZnO-based solar cells. Chlorophylls (Chls) are key photosynthetic pigments in natural photosynthetic systems; their functions include harvesting light and transferring energy and electrons [26,27]. Due to the advantageous light-harvesting capability of Chls and their derivatives, they have been introduced into DSSCs as dye sensitizers [28–31]. The most efficient Chl *a* derivative – methyl *trans*-3^2-carboxypyropheophorbide *a* (chlorin 2, see Fig. 1), which has an extended π-conjugation length along the Q_y axis of the chlorin skeleton – was recently synthesized and gave a similar IPCE as ruthenium complex N719 [31]. Compared to the relatively acidic dye solution of ruthenium complexes N3 and N719, chlorin 2 has only one carboxy group more favorable to ZnO, so there should be less of a chance for aggregation of the dye molecules during the dye upload process. There is also one conjugated double bond space between the chlorin macrocycle and the carboxy group, suggesting more complicated binding modes. Therefore, chlorin 2 should be able to anchor to TiO_2 and ZnO surfaces through different modes.

In the present paper, we fabricated DSSCs using chlorin 2 as a dye sensitizer and nanocrystalline TiO_2 and ZnO with identical particle sizes as semiconductor electrodes. The binding modes of the dye–TiO_2 and dye–ZnO systems were studied using attenuated total reflectance-Fourier transform infrared (ATR-FTIR) measurements. Moreover, by using density functional theory (DFT) calculations based upon system models, we investigated which binding mode is preferable for dye–TiO_2 and dye–ZnO. In order to confirm the reliability of the computational models and clarify the results of photovoltaic performance of these DSSCs, we applied time-dependent DFT (TD-DFT) calculations to the dye–TiO_2 and dye–ZnO system models. The TD-DFT results were further decomposed by transition-component analysis (TCA) [32] to produce more information on the difference between the two semiconductors. The lower photocurrent of the ZnO-based solar cell was discussed based upon the TD-DFT calculations and the main frontier orbitals constituting the main configurations. The lower open-circuit photovoltage (V_{oc}) value of the ZnO-based solar cell was discussed using the observed data of the electron lifetime (τ) and electron diffusion coefficient (D).

2. Experimental

2.1. Synthesis and computational

The synthesis of chlorin 2 was described previously [31].

The calculated IR spectra are based upon optimized structures (by TD-DFT) with the scaling factor of 93% due to neglect of anharmonicity in the real system. All calculations were done using Gaussian 03 with the AIST super cluster in Tsukuba and the Research Center for Computational Science in Okazaki.

2.2. Preparation of semiconductor films

The TiO_2 nanocrystalline film with 20-nm particle size was prepared by spreading TiO_2 paste (Solaronix nanooxide-T20) on FTO glass (Nippon Sheet Glass 10 $\Omega\,cm^{-2}$). After sintering at 450 °C for 30 min, a second layer of TiO_2 with 300-nm particle size (CR-EL, Ishihara Industry) was spread using the same method, followed by treatment with a $TiCl_4$ aqueous solution (Wako chemicals). The double-layered paste was finally sintered at 450 °C for 30 min before dyeing in an ethanol solution of chlorin 2 (3×10^{-4} M). The ZnO paste with 20-nm particle size was prepared by mixing 2 g ZnO powder (Finex-50, Sakai Chemical Industry), 1 g polyethylene glycol (MW = 20,000, Wako Chemicals), 0.5 g hydroxypropyl cellulose (TCI), and 8 g distilled water. The ZnO paste for light scattering was prepared using a similar method as the 20-nm paste, but with a 300-nm ZnO powder (Microsized-ZnO, Sakai Chemical Industry) instead. The thickness of the TiO_2 (ZnO) film was ~8 μm for the 20-nm particle size and ~4 μm for the 300-nm particle size. The ZnO pastes were sintered at 450 °C for 8 min without further treatment with $TiCl_4$.

2.3. Spectroscopic characterizations

The UV–vis absorption spectra were measured with a Shimadzu UV-3150 spectrometer. ATR-FTIR measurements were carried out using a Jasco FT/IR 6200 spectrometer. The τ and D values were measured using a SLIM-PCV (PSL-100, EKO, Japan) with a stepped laser beam (YL-331M, Yamamoto Photonics, Japan). The photovoltaic measurements were conducted using a Xe lamp as a light source to simulate the AM 1.5 spectrum (Wacom, WXS-80C-3, 100 $mW\,cm^{-2}$). The incident light intensity was calibrated with a standard solar cell for amorphous silicon solar cells produced by the Japan Quality Assurance Organization. The IPCE profile of each DSSC was recorded under monochromatic irradiation by use of a setup for IPCE measurements (PEC-S2012, Peccell), consisting of

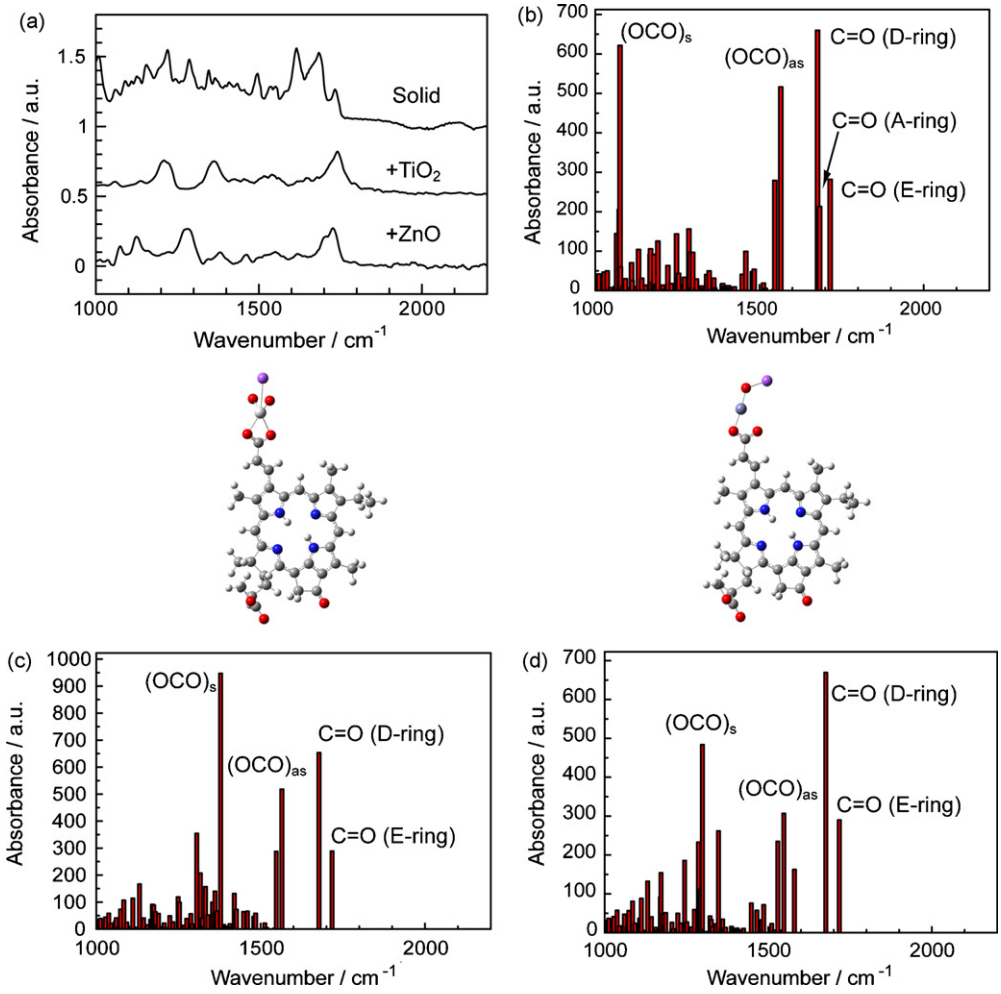

Fig. 2. (a) The ATR-FTIR spectra of free chlorin 2 as a powder and deposited on TiO_2 and ZnO electrodes, and the calculated IR spectra of chlorin 2 as (b) free powder, (c) covalently bound with TiO_2Na in bidentate chelating mode, and (d) covalently bound with ZnONa in monodentate mode.

a 150-W Xe lump and a monochrometer (Instruments S.A. Triax 180).

2.4. Fabrication of dye-sensitized solar cells

Each DSSC was fabricated using a semiconductor electrode with 0.25 cm^2 working area, a counter electrode of Pt-sputtered FTO glass (Nippon Sheet Glass 10 $\Omega\,cm^{-2}$), and an electrolyte containing 0.1 M LiI, 0.05 M I_2, 0.6 M 1-propyl-3-methylimidazolium iodide, and 0.5 M *tert*-butylpyridine in a mixture of acetonitrile and valeronitrile (1:1, v/v).

3. Results and discussion

3.1. Chlorophyll a derivative bound to TiO_2 and ZnO surface with different binding modes

At present, chlorin 2 has the best performance as a chlorophyllous sensitizer for DSSCs [31]. A comparison of chlorin 2 with other chlorin sensitizers suggests that the LUMO + 2 orbital of the former is a key orbital for electron injection. Clarifying how the LUMO + 2 orbital works upon binding to the semiconductor surface is necessary.

In order to understand how the chlorin 2 molecule is bound to the TiO_2 and ZnO surface, the ATR-FTIR spectra for the dye sensitizer in crystalline form and on the TiO_2 and ZnO particles were measured as shown in Fig. 2a–d show the calculated IR spectra of chlorin 2 alone, chlorin 2–TiO_2Na, and chlorin 2–ZnONa, respectively. Fig. 2c and d also depicts the optimized structures of the system models chlorin 2–TiO_2Na and chlorin 2–ZnONa respectively over their estimated spectra. In the calculated models, the former prefers the bidentate chelating mode and the latter prefers the monodentate mode. The semiconductor particles are constructed by many molecules of the same kind. Here, we use a Na ion to describe the semiconductor crystal except for the one directly interacting with the dye sensitizer. All the systems were optimized through DFT calculations with the B3LYP exchange correlations function [33,34] and the 6-31G(d,p) [35] basis set for HCNONa and TZVP [36] for Ti and Zn in Gaussian 03. [37] Although the modeling of the semiconductor component by TiO_2Na and ZnONa systems was so limited, TD-DFT [38] calculations for these systems reproduced the experimental absorption spectra very well and is discussed below.

We think our calculated IR spectrum, based upon these relatively small system models, can be used to characterize the experimental IR spectrum for the dye attached to TiO_2 and ZnO particles after appropriate scaling due to neglect of the anharmonicity in the real system. For our purposes, we used 93% following the recommendation by Sinha et al. [39].

According to the measured ATR-FTIR spectrum in Fig. 2a, the solid sample of chlorin 2 has aggregate as a major morphology; this means that the calculated spectrum of one molecule *in vacuo* produces big mismatches with the observed spectrum. The following is only a rough assignment of signals free from the aggregate

effect, as further discussion on the IR spectrum of aggregated dye is not a major component of this paper:

1. The peak at the wavenumber 1735 cm^{-1} corresponds to the C═O stretching modes for the E-ring, while the peak at 1615 cm^{-1} does not correspond to the D-ring but probably to the C═C stretching of the chlorin macrocycle.
2. The peak at 1684 cm^{-1} corresponds to the C═O stretching mode for the COOH group at the A-ring.
3. The peaks at 1220 and 1596 cm^{-1} correspond to the symmetric $\nu(COO)_s$ and asymmetric $\nu(COO)_{as}$ modes anchoring the COO portion.
4. The peak at 1286 cm^{-1} corresponds to the C–O stretching mode.

Fig. 2a shows that when the dye sensitizer was deposited on the TiO_2 film, the COOH peak disappeared and three new peaks at 1209, 1359, and 1539 cm^{-1} appeared. Fig. 2c shows the calculated IR spectrum of the chlorin 2–TiO_2Na system with bidentate chelating binding between dye and TiO_2. The positions of the new peaks at 1359 and 1539 cm^{-1} correspond nicely to the calculated symmetric $\nu(COO)_s$ and asymmetric $\nu(COO)_{as}$ modes respectively for 3^2-COO–TiO_2Na. In comparison to the IR spectrum for the dye–TiO_2 system, the IR spectrum for dye–ZnO shows only two additional peaks at 1278 and 1550 cm^{-1}. Fig. 2d shows the calculated IR spectrum for the chlorin 2–ZnONa system; it is similar to the chlorin 2–TiO_2Na system but for the monodentate mode. The two peaks assigned to the $\nu(COO)_s$ and $\nu(COO)_{as}$ modes are based on a comparison of the corresponding peaks in the calculated spectrum shown in Fig. 2d.

The splitting of the carboxylate stretching modes ($\Delta = \nu(COO)_{as} - \nu(COO)_s$) is a key factor in distinguishing the different binding modes in dye–metal systems [19]. The Δ value for monodentate mode has been found to be larger than that for the bidentate chelating and bridging modes. The validity of the above calculations is also supported by this theory. The fact that the observed Δ value for chlorin 2–TiO_2 was 180 cm^{-1} – much smaller than the value for chlorin 2–ZnO at 272 cm^{-1} – strongly supports our assignment of binding modes.

In Fig. 2a, the experimental IR spectrum for chlorin 2–TiO_2 has another new peak at 1209 cm^{-1}. If chlorin 2–TiO_2 has the monodentate mode – which unfortunately cannot be described by a single optimized structure – the peak can be explained due to the longer bond length for Ti–O than Zn–O. Therefore, the experimental IR spectrum at room temperature suggests both bidentate chelating and monodentate modes for chlorin 2–TiO_2.

Fig. 3a shows the absorption spectra of chlorin 2 deposited on TiO_2 and ZnO nanocrystalline films with the same particle size of 20 nm. The two spectra were similar except for the ratio of the Soret and Q bands intensities; this was larger in TiO_2 but smaller in ZnO. The IR spectra suggest that this difference is due to the intrinsic binding properties of the dye sensitizer on the two different semiconductors. Fig. 4 shows the theoretical absorption spectra and oscillator strength for (a) chlorin 2–TiO_2Na and (b) chlorin 2–ZnONa. Tables 2 and 3 summarize the main configurations of the theoretical absorption spectra. The two spectra were similar except for the ratio of the Soret and Q bands intensities; they are consistent with the experimental absorption spectra shown in Fig. 3a. The results of the calculated absorption spectra also support the validity of the above binding modes.

3.2. Photovoltaic performances of chlorophyll a derivative-sensitized TiO_2- and ZnO-based solar cells

Fig. 3b shows the IPCE and Fig. 3c shows the photocurrent-photovoltage curves (*I–V* curves) of the TiO_2- and ZnO-based solar cells sensitized with chlorin 2. Table 1 lists the relative parameters

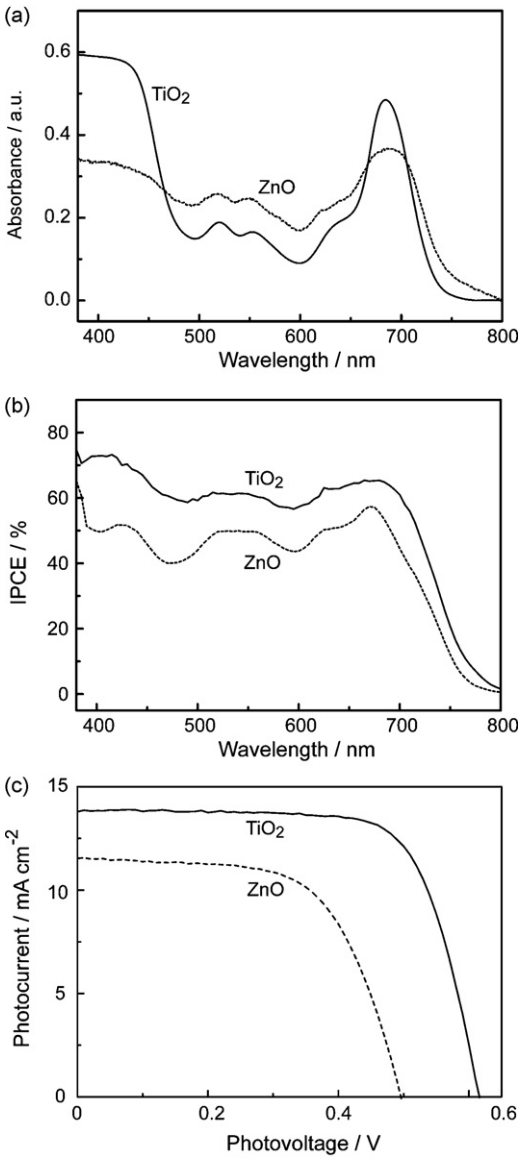

Fig. 3. (a) The electronic absorption spectra of the dye deposited on TiO_2 and ZnO films, (b) the IPCE profiles, and (c) the *I–V* curves of DSSCs based upon chlorin 2-sensitized TiO_2 and ZnO electrodes.

obtained from the *I–V* curves. The shape of the IPCE profiles nicely corresponds to the absorption spectra. The IPCE values of the ZnO solar cell for each wavelength are always less than those of the TiO_2 solar cell. As an integrated IPCE profile under the solar energy spectrum, the photocurrent in the *I–V* curve for the ZnO solar cell is also less than that for TiO_2 solar cell. The ZnO solar cell sensitized with chlorin 2 gives a V_{oc} value of 0.50 V, which is 0.11 V smaller than the V_{oc} value of 0.61 V for the TiO_2 solar cell. As a result, the η value

Table 1
The photovoltaic performance of chlorin 2-sensitized TiO_2- and ZnO-based solar cells – including the short-circuit photocurrent (J_{sc}), open-circuit photovoltage (V_{oc}), fill factor (FF), and energy-to-electricity conversion efficiency (η) – and the energy levels of the conduction band (E_{CB}) and band gap (E_g) for the two different kinds of semiconductors. These photovoltaic parameters were measured under AM 1.5 (100 mW cm^{-2}) illumination.

Semiconductor	J_{sc} (mA cm^{-2})	V_{oc} (V)	FF	η (%)	E_{CB} (eV)	E_g (eV)
TiO_2	13.8	0.61	0.72	6.1	−4.21	3.20
ZnO	11.5	0.50	0.62	3.6	−4.19	3.20

Table 2
The TD-DFT (B3LYP/6-31G(d,p) for HCNONa and TZVP for Ti) results for the transition energies (λ in nm) and oscillation strengths (*f* in a.u.) for chlorin 2–TiO_2Na.

	Main configurations (|C| > 0.2) [HOMO (181): LUMO (182)]	λ	*f*
1	0.59 (181 → 182) −0.35 (180 → 183)	600	0.228
2	0.58 (180 → 182) +0.36 (181 → 183)	554	0.069
3	0.67 (179 → 182)	440	0.006
4	0.52 (180 → 183) +0.22 (179 → 183) +0.20 (180 → 185)	412	0.588
5	0.49 (181 → 183) +0.27 (181 → 185) +0.21 (180 → 185)	412	0.291
6	0.66 (177 → 182)	409	0.003

Table 3
The TD-DFT (B3LYP/6-31G(d,p) for HCNONa and TZVP for Zn) results for the transition energies (λ in nm) and oscillation strengths (*f* in a.u.) for chlorin 2–ZnONa.

	Main configurations (|C| > 0.2) [HOMO (181): LUMO (182)]	λ	*f*
1	0.59 (181 → 182) −0.36 (180 → 183)	590	0.208
2	0.57 (180 → 182) +0.38 (181 → 183)	543	0.047
3	0.69 (179 → 182)	518	0.006
4	0.70 (178 → 182)	496	0.000
5	0.68 (179 → 184)	483	0.021
6	0.68 (178 → 184)	433	0.033
7	0.68 (177 → 182)	425	0.002
8	0.70 (181 → 184)	414	0.000
9	0.44 (179 → 183) −0.41 (180 → 183)	404	0.365
10	0.66 (175 → 182)	403	0.001

for the ZnO solar cell is 3.6%, which is less than that of the TiO_2 solar cell at 6.1%.

3.3. The origin of the lower performance at ZnO-based solar cell

In order to explain the lower values for the short-circuit photocurrent (J_{sc}) and the V_{oc} of the ZnO solar cell sensitized with chlorin 2, we executed DFT calculations for the chlorin 2–TiO_2Na and chlorin 2–ZnONa systems. As described previously, the optimal binding structures for these two systems are the bidentate chelating and monodentate binding modes, respectively. Since the bidentate chelating mode strongly connects the dye with semiconductor, the calculation results explained very well the experimental IR data and superiority of the TiO_2 solar cell.

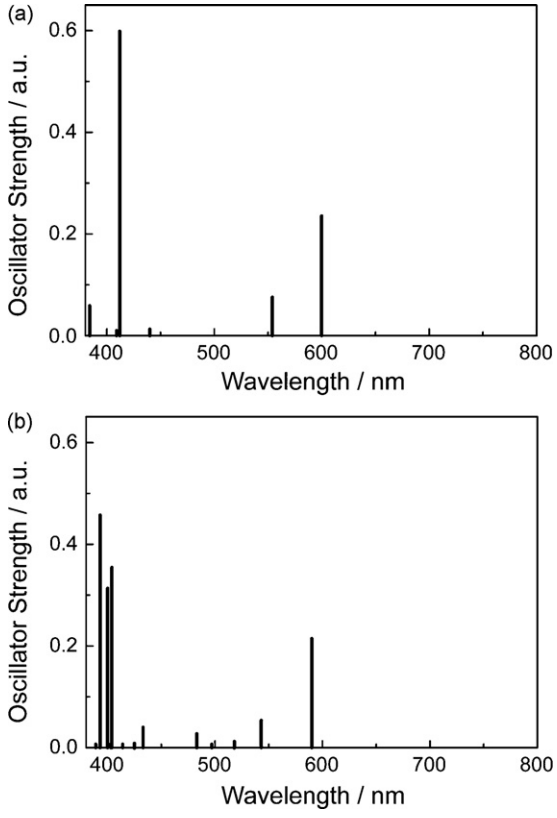

Fig. 4. Theoretical absorption spectra and oscillator strength, based upon TD-DFT/B3LYP/6-31G(d,p) for HCNONa and TZVP for Ti and Zn, for (a) chlorin 2–TiO_2Na and (b) chlorin 2–ZnONa.

We also performed TD-DFT calculations on these two systems with the results summarized in Tables 2 and 3. Fig. 5 shows the results of the frontier Kohn–Sham orbitals for chlorin 2–TiO_2Na (Fig. 5a) and chlorin 2–ZnONa (Fig. 5b) based upon the DFT calculations; here, the LUMO + 2 of chlorin 2–TiO_2Na is not shown, because this orbital does not participate in any electron transitions as listed in Table 2. The HOMO-1, HOMO, LUMO, LUMO + 1 orbitals of Fig. 5a are similar to those of Fig. 5b, respectively, while the rest of the orbitals, especially the HOMO-2 and LUMO + 3 of chlorin 2–TiO_2Na are definitely different with the HOMO-2 and LUMO + 2 of chlorin 2–ZnONa. No electron is present in the chromatophore portion of HOMO-2 and LUMO + 2 for chlorin 2–ZnONa with a monodentate binding mode. Thus, except for reverse electron transfer, no other kind of positive electron transfer takes place through the use of these particular orbitals. The LUMO + 2 orbital of chlorin 2, which here corresponds to LUMO + 3 of chlorin 2–TiO_2Na, is very efficient at electron injection, as suggested by the previous investigation [31]. A reduced photocurrent can naturally be expected in the chlorin 2–ZnONa system. In this system, the Soret band (9th in Table 3) includes an electron leak from the semiconductor to the dye. On the other hand, in chlorin 2–TiO_2Na system, the Soret bands (4th and 5th in Table 2) account for the good electron injection from the dye to the semiconductor using the LUMO + 3 orbital. These calculation data are consistent with the experimental IPCE shown in Fig. 3b.

For deeper understanding of the difference between the system models of the chlorin 2–TiO_2Na and chlorin 2–ZnONa systems, we employed TCA to decompose the TD-DFT calculations. TCA was recently proposed [32] and used to analyze the calculated absorption spectra based on TD-DFT and quantitatively summarize the contents of several types of electron transfer which accompany electron photo-excitation; these are described with pairs of the initial and final parts. The TCA based on TD-DFT calculations can be used to analyze the calculated absorption spectra and quantitatively summarize the contents of several types of electronic transitions in Ru polypyridyl dye molecules associated with photoexcitation [32,40]. These results successfully confirmed that theoretical analysis of the absorption spectra using the TCA method

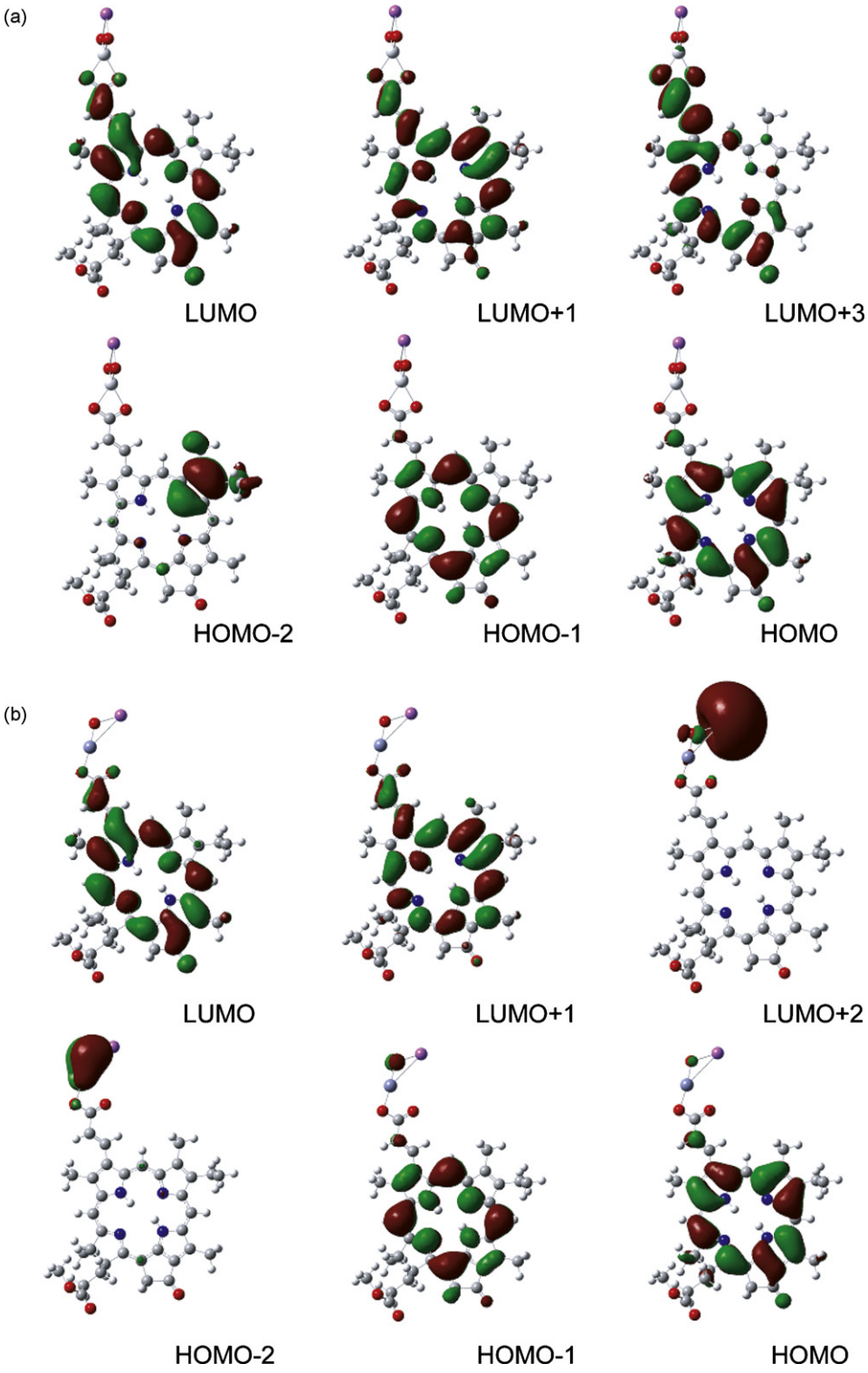

Fig. 5. The frontier molecular orbitals of (a) chlorin 2 covalently bound with TiO_2Na in bidentate chelating mode and (b) chlorin 2 covalently bound with ZnONa in monodentate mode.

is useful for interpreting electron transfer behavior for TD-DFT calculations.

Fig. 6 describes the TCA results for the (a) chlorin 2–TiO_2Na and (b) chlorin 2–ZnONa systems. As per the procedure for TCA, first the absorption spectra were simulated by the Gaussian convolution $\sigma = 0.0786$ eV, which corresponds to the full-width at half maxima of 1500 cm^{-1} used for free-base *N*-confused porphine [41]. The black curves are the results. Next, the total curves were decomposed to each group component: (chlorin 2 → chlorin 2) (red), (chlorin 2 → semiconductor) (blue), and (semiconductor → chlorin 2) (green).

In Fig. 6, the red curves are due to electron excitation inside chlorin 2 and reproduce the experimental results well; the ratio of Soret and Q band intensities are larger in TiO_2 but smaller in ZnO. The blue curves are due to the fast electron injection from the chlorin 2 dye to the semiconductor, and the green curves are due to the

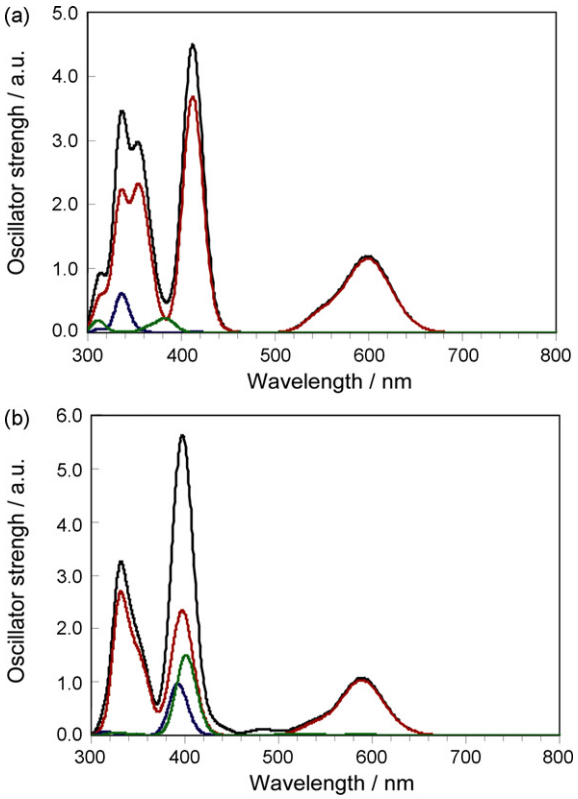

Fig. 6. The TCA of the TD-DFT results for (a) chlorin 2–TiO_2Na and (b) chlorin 2–ZnO. The black curves are due to the total TD-DFT results; each group component is (chlorin 2 → chlorin 2) (red), (chlorin 2 → semiconductor) (blue), and (semiconductor → chlorin 2) (green). (For interpretation of the references to color in this figure legend, the reader is referred to the web version of the article.)

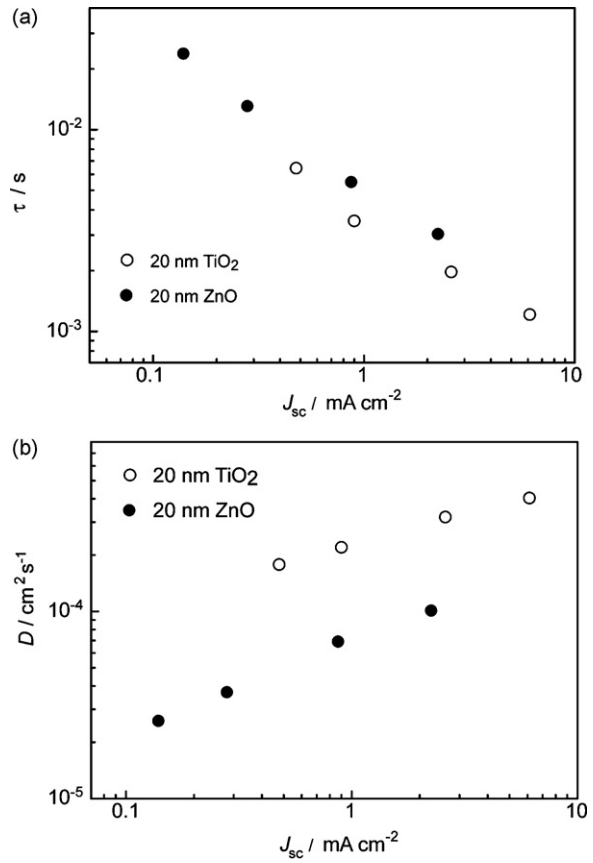

Fig. 7. (a) The J_{sc}-dependent τ and (b) D of DSSCs based upon chlorin 2-sensitized TiO_2 (open circles) and ZnO electrodes (closed circles).

fast back electron leak from the semiconductor to the chlorin 2 dye. At the wavelength of 400 nm in Fig. 6b, neither the blue nor green peak portions are negligible. These results are understandable due to the strong correlation of ZnO with chlorin 2 and consistent with the lower η for the ZnO cell than the TiO_2 cell.

Fig. 7 shows the results for the measured τ and D values of DSSCs based upon the chlorin 2-sensitized TiO_2 and ZnO electrodes by the use of the stepped light-induced transient measurement of photocurrent and voltage method (SLIM-PCV) [42]. The τ value of the ZnO solar cell is slightly larger than that of the TiO_2 solar cell and correlates well with the observations based upon the ruthenium complex N719 [17], suggesting a reduced charge recombination process between the ZnO semiconductor and I^-/I_3^- in the electrolyte. We can therefore conclude that the lower V_{oc} value of ZnO does not originate from the charge recombination process. In Fig. 7b, the D value is significantly larger in the TiO_2 solar cell. Electron transportation in the film contains only two steps: trapping in each nanoparticles and crossing barriers between neighboring nanoparticles. For bulk semiconductor materials, ZnO is well known to have higher electron mobility than TiO_2; this principle can be applied to each particle of the nanocrystalline film in the present case. A smaller D value in the ZnO solar cell can only be due to the inefficient electron diffusion between each ZnO nanoparticle. This means that the electrons have to possibly cross barriers with larger energy gaps in the ZnO films. The larger energy gap as a barrier between individual ZnO nanoparticles is mainly due to a less crystalline conformation of nanostructures. As far as we know, the V_{oc} value in a DSSC is determined by the difference in energy levels for the quasi-Fermi level of the semiconductor and the redox species in the electrolyte. The difference in the V_{oc} value should be probably originated from the different interaction of FTO conductive glass with TiO_2 or ZnO, through so called Fermi level pinning effect.

4. Conclusion

We applied chlorin 2, a chlorophyll *a* derivative, to DSSCs based upon TiO_2 and ZnO nanocrystalline electrode materials. The TiO_2-based solar cell gives higher J_{sc}, V_{oc}, and η values compared to those for the ZnO-based solar cell. ATR-FTIR measurements for the dye-sensitized semiconductor electrodes suggest that the dye sensitizer is bound to TiO_2 with both the bidentate chelating and monodentate modes, while it is predominantly bound to ZnO with the monodentate mode. The experimental IR spectra consist of the optimal structures based upon DFT calculations: the dye sensitizer is bound to TiO_2 with the bidentate chelating mode, while it is bound to ZnO with the monodentate mode. TCA, based upon the TD-DFT results, explained very well the experimental UV–vis spectra and the difference in η values between the DSSCs based on TiO_2 and ZnO nanocrystalline electrode materials.

Acknowledgements

The calculations were done using the AIST super cluster in Tsukuba and the Research Center for Computational Science in Okazaki. This work was partially supported by Grants-in-Aid for Young Scientists (B) (Nos. 20760606 and 21750154) (to X.F.W. and S.S.) from the Ministry of Education, Culture, Sports, Science, and Technology (MEXT) of Japan and Grants-in-Aid for Scientific Research (B) (No. 19350088) (to H.T.) from the Japan Society for the Promotion of Science (JSPS).

Appendix A. Supplementary data

Supplementary data associated with this article can be found, in the online version, at doi:10.1016/j.jphotochem.2010.01.004.

References

[1] B. O'Regan, M. Grätzel, Nature 353 (1991) 737.
[2] M. Grätzel, Nature 414 (2001) 338.
[3] Y. Chiba, A. Islam, Y. Watanabe, R. Komiya, N. Koide, L. Han, Jpn. J. Appl. Phys. 45 (2006) L638.
[4] M.K. Nazeeruddin, F.D. Angelis, S. Fantacci, A. Selloni, G. Viscardi, P. Liska, S. Ito, B. Takeru, M. Grätzel, J. Am. Chem. Soc. 127 (2005) 16835.
[5] M.A. Butler, D.S. Ginley, J. Mater. Sci. 15 (1980) 1.
[6] H. Tsubomura, M. Matsumura, Y. Nomura, T. Amamiya, Nature 261 (1976) 402.
[7] M. Izaki, T. Omi, Appl. Phys. Lett. 68 (1996) 2439.
[8] K. Kakiuchi, E. Hosono, S. Fujihara, J. Photochem. Photobiol. A 179 (2006) 81.
[9] T.W. Hamann, A.F. Martinson, J.W. Elam, M.J. Pellin, J.T. Hupp, Adv. Mater. 20 (2008) 1560.
[10] T.P. Chou, Q. Zhang, G.E. Fryxell, G.Z. Cao, Adv. Mater. 19 (2007) 2588.
[11] E. Hosono, S. Fujihara, I. Honna, H.S. Zhou, Adv. Mater. 17 (2005) 2091.
[12] Q. Zhang, T.P. Chou, B. Russo, S.A. Jenekhe, G. Cao, Angew. Chem. Int. Ed. 47 (2008) 2402.
[13] M. Saito, S. Fujihara, Energy Environ. Sci. 1 (2008) 280.
[14] K. Keis, J. Lindgren, S. Lindquist, A. Hagfeldt, Langmuir 16 (2000) 4688.
[15] K. Keis, E. Magnusson, H. Lindstrom, S.E. Lindquist, A. Hagfeldt, Sol. Energy Mater. Sol. Cells 73 (2002) 51.
[16] T.P. Chou, Q. Zhang, G. Cao, J. Phys. Chem. C 111 (2007) 18804.
[17] M. Quintana, T. Edvinsson, A. Hagfeldt, G. Boschloo, J. Phys. Chem. C 111 (2007) 1035.
[18] J.M. Szarko, A. Neubauer, A. Bartelt, L. Socacius-Siebert, F. Birkner, K. Schwarzburg, T. Hannappel, R. Eichberger, J. Phys. Chem. C 112 (2008) 10542.
[19] K.S. Finnie, J.R. Bartlett, J.L. Woolfrey, Langmuir 14 (1998) 2744.
[20] M.K. Nazeeruddin, R. Humphey-Baker, D.L. Officer, W.M. Campbell, A.K. Burrell, M. Grätzel, Langmuir 20 (2004) 6514.
[21] R. Zhang, J. Pan, E.P. Briggs, M. Thrash, L.L. Kerr, Sol. Energy Mater. Sol. Cells 92 (2008) 425.
[22] J. Rochford, E. Galoppini, Langmuir 24 (2008) 5366.
[23] Y.X. Weng, L. Li, Y. Liu, L. Wang, G.Z. Yang, J. Phys. Chem. B 107 (2003) 4356.
[24] H. Minoura, T. Yoshida, Electrochemistry 76 (2008) 109.
[25] T. Yoshida, J. Zhang, D. Komatsu, S. Sawatani, H. Minoura, T. Pauportė, D. Lincot, T. Oekermann, D. Schlettwein, H. Tada, D. Wöhrle, K. Fimanolo, M. Matsui, H. Miura, H. Yanagi, Adv. Funct. Mater. 19 (2009) 17.
[26] H. Scheer, in: B. Grimm, R.J. Porra, W. Rüdiger, H. Scheer (Eds.), Advances in Photosynthesis and Respiration, vol. 25, Springer, Dordrecht, 2006 (Chapter 1).
[27] H. Tamiaki, R. Shibata, T. Mizoguchi, Photochem. Photobiol. 83 (2007) 152.
[28] X.-F. Wang, C.H. Zhan, T. Maoka, Y. Wada, Y. Koyama, Chem. Phys. Lett. 447 (2007) 79.
[29] X.-F. Wang, Y. Koyama, Y. Wada, S. Sasaki, H. Tamiaki, Chem. Phys. Lett. 439 (2007) 115.
[30] X.-F. Wang, Y. Koyama, H. Nagae, Y. Wada, S. Sasaki, H. Tamiaki, J. Phys. Chem. C 112 (2008) 4418.
[31] X.-F. Wang, O. Kitao, H. Zhou, H. Tamiaki, S. Sasaki, Chem. Commun. 45 (2009) 1523.
[32] O. Kitao, H. Sugihara, Inorg. Chim. Acta 361 (2008) 712.
[33] A.D. Beck, J. Chem. Phys. 98 (1993) 5648.
[34] C. Lee, W. Yang, R.G. Parr, Phys. Rev. B 37 (1988) 785.
[35] R. Ditchfield, W.J. Hehre, J.A. Pople, J. Chem. Phys. 54 (1971) 724.
[36] A. Schaefer, H. Horn, R. Ahlrichs, J. Chem. Phys. 97 (1992) 2571.
[37] M.J. Frisch et al., Gaussian 03, Revision C.02, see Supporting information.
[38] R.E. Stratmann, G.E. Scuseria, M.J. Frisch, J. Chem. Phys. 109 (1998) 8218.
[39] P. Sinha, S.E. Boesch, C. Gu, R.A. Wheeler, A.K. Wilson, J. Phys. Chem. A 108 (2004) 8213.
[40] O. Kitao, Electrochemistry 76 (2008) 165.
[41] S. Vyas, C.M. Hadad, D.A. Modarelli, J. Phys. Chem. A 112 (2008) 6533.
[42] S. Nakade, T. Kanzaki, Y. Wada, S. Yanagida, Langmuir 21 (2005) 10803.